Core Control Principles of the Eukaryotic Cell Cycle

Souradeep Basu (saz.basu@crick.ac.uk)
The Francis Crick Institute
Paul Nurse
The Francis Crick Institute
Andrew Jones
Francis Crick Institute

Biological Sciences - Article

Keywords:

Posted Date: October 27th, 2021

DOI: https://doi.org/10.21203/rs.3.rs-1008929/v1

Abstract

Cyclin dependent kinases (CDKs) lie at the heart of eukaryotic cell cycle control, with different Cyclin-CDK complexes initiating DNA replication (S-CDKs) and mitosis (M-CDKs). However, the principles on which Cyclin-CDKs organise the temporal order of cell cycle events are contentious. The currently most widely accepted model, is that the S-CDKs and M-CDKs are functionally specialised, with significant different substrate specificities to execute different cell cycle events. A second model is that S-CDKs and M-CDKs are redundant with each other, with both acting as sources of overall cellular CDK activity. Here we reconcile these two views of core cell cycle control. Using a multiplexed phosphoproteomics assay of in vivo S-CDK and M-CDK activities in fission yeast, we show that S-CDK and M-CDK substrate specificities are very similar, showing that S-CDKs are not completely specialised for S-phase alone. Normally S-CDK cannot undergo mitosis, but is able to do so when Protein Phosphatase 1 (PP1) is removed from the centrosome, allowing several mitotic substrates to be better phosphorylated by S-CDK in vivo. Thus, an increase in S-CDK activity in vivo is sufficient to allow S-CDK to carry out M-CDK function. Therefore, we unite the two opposing views of cell cycle control, showing that the core cell cycle engine which temporally orders cell cycle progression is largely based upon a quantitative increase of CDK activity through the cell cycle, combined with minor qualitative differences in catalytic specialisation of S-CDKs and M-CDKs.

Introduction

The core CDK eukaryotic cell cycle control system is based on S-phase and mitosis being controlled by CDKs complexed with S-phase cyclins (S-CDKs) and mitotic cyclins (M-CDKs), respectively[3,4]. However, there are two fundamentally different views as to how this core CDK system brings about the temporal order of cell cycle events[1]. The first is that the correct cell cycle ordering and execution of S-phase and mitosis is the consequence of major qualitative differences in the biochemical activities of the S-CDK and M-CDK complexes due to different cyclins[2,5,6]. These CDKs appear sequentially, and target different substrates to successively drive S-phase and mitosis[5,6]. The second view emphasises the importance of the total quantitative level of CDK activity in the cell, contributed by both S-CDK and M-CDK, with increasing activity driving the ordering of S-phase and mitosis[7,8]. This comes about because S-phase substrates are phosphorylated at a lower total CDK activity than mitotic substrates[9].

However, neither of these models are satisfactory to explain core CDK control. If major qualitative differences in CDK complexes bring about cell cycle order, then S-CDKs and M-CDKs should be indispensable as they carry out distinct tasks, but in fact S-CDKs can be deleted in a range of eukaryotes and cell cycle order is still maintained[10-16]. This is consistent with the alternative quantitative hypothesis, but that view predicts that since both S-CDK and M-CDK provide similar CDK activities they should be interchangeable. However, S-CDKs are unable to fully compensate for M-CDKs and complete mitosis[17-21]. Here we investigate core CDK control in fission yeast and provide a reconciliation of these opposing views, demonstrating the principles upon which the eukaryotic cell cycle is organised.

Results

S-CDK can initiate mitosis but not complete it

In the fission yeast, the S-CDK consists of Cdk1 (encoded by *cdc2*) complexed with the S-phase cyclin Cig2, and the M-CDK consists of Cdk1 complexed with the M-cyclin Cdc13. It has been well established that Cdc13-Cdk1 (M-CDK) can compensate for Cig2-Cdk1 (S-CDK)[7], but it is not clear if S-CDK can compensate for M-CDK. Early studies using a temperature sensitive *cdc13* mutant showed that Cig2-Cdk1 could initiate mitosis could not complete it[17,18], although a more recent study using the temperature sensitive *cdc13-G282D*, has suggested that Cig2-Cdk1 can completely compensate for Cdc13-Cdk1[22]. However, the authors of this study cautioned that this temperature sensitive mutant might not have eliminated all the M-CDK activity from the cell, a potential problem because they reported *cdc13-G282D* cells accumulated dividing septated cells at their restrictive temperature, suggesting that mitoses were taking place. To re-examine if the S-CDK is able to overcome loss of M-CDK function, we expressed the S-phase cyclin Cig2 in the strong temperature sensitive mutant *cdc13-9* and observed that, at the *cdc13-9* restrictive temperature, mitosis was completely blocked (Extended data Figure 1), indicating that Cig2 cannot compensate for Cdc13 for the execution of mitosis.

To investigate further the interchangeability of S- and M-CDKs, we constructed two monomeric S-CDK or M-CDK fusion proteins covalently tagged with Superfolder GFP (sfGFP) under control of a tetracycline-inducible promoter (Figure 1a). Endogenous CDK activity was removed using a temperature-sensitive Cdk1 mutant (*cdk1-ts*) which completely inhibited CDK substrate phosphorylation and blocked cell-cycle progression at 36 ^{o}C (Extended data Figure 2). We combined this with a mitotic CDK activity biosensor, synCut3-mCherry, which translocates from the cytoplasm into the nucleus at mitosis due to direct CDK phosphorylation (Figure 1b)[23].

Endogenous CDK activity was removed by shifting cells to 36 ^{o}C for two hours, and the S-CDK and M-CDK fusion proteins were induced by tetracycline addition (Figure 1c). M-CDK and S-CDK were similarly expressed and accumulated in the nucleus of cells (Figure 1d-g). Both CDKs resulted in import of synCut3 into the nucleus, indicating that sufficient CDK activity was attained to enable mitotic entry (Figure 1f,g). Following this, M-CDK expressing cells were able to form spindles, degrade M-CDK, export synCut3-mCherry from the nucleus, and undergo nuclear separation (Figure 1f,h,i). In contrast, cells expressing S-CDK were unable to construct spindles, export synCut3 from the nucleus, or degrade the Cyclin-CDK (Figure 1g,h,j), and generated aberrant or incomplete mitotic and cell division events as compared with M-CDK (Figure 1i,j). The ability of S-CDK and M-CDK to trigger mitotic events was dependent on CDK activity, as kinase dead S-CDK and M-CDK were unable to cause mitotic events despite high CDK expression (Extended data figure 3). We conclude that unlike M-CDK, S-CDK is unable to complete mitosis, but is capable of bringing about the initial stages of mitotic entry.

Global *in vivo* Cyclin-CDK specificity

That S-CDK cannot substitute for M-CDK for the completion of mitosis and cell division is compatible with a qualitative view of CDK cell cycle control, with the S-CDK being unable to phosphorylate essential mitotic substrates. This suggests there are substrates which are poorly phosphorylated by S-CDK compared with M-CDK *in vivo*. To investigate this, we developed a time-resolved multiplexed proteomics and phosphoproteomics procedure to monitor both the amount of Cyclin-CDK present in cells and the ability of that CDK to phosphorylate hundreds of known CDK substrates[9], allowing us to assay the activity of S-CDK and M-CDK *in vivo*. We expressed S-CDK and M-CDK fusion protein variants lacking the APC/C destruction box (ΔDB) motifs in the absence of endogenous CDK activity. These Cyclin-CDK variants are not destroyed by the cyclin destruction machinery, and are thus stably expressed (Extended data figure 4). The levels of S-CDK and M-CDK were monitored using proteomics, and the phosphorylation status of hundreds of CDK substrates were quantified using multiplexed phosphoproteomics in response to increasing S-CDK or M-CDK level.

Both complexes were produced similarly after induction (Extended data figure 4), and phosphorylation was normalised to the maximum phosphorylation levels detected in the experiments. 280 previously identified CDK phosphosites became phosphorylated, and were clustered based on their behaviour in response to S-CDK and M-CDK activity (Figure 2a, Table S1). Four distinct phosphorylation behaviours were observed. The largest group of 180 CDK phosphorylation events (Cluster 1, ~64%) displayed essentially identical phosphorylation responses to both S-CDK or M-CDK, reaching identical average maximum phosphorylation levels with similar phosphorylation dynamics (Figure 2a,b,c). Clusters 2 and 4 together contain 60 phosphorylation events (~21%) that were preferentially phosphorylated by S-CDK, despite most being mitotic substrates (Figure 2a,b,c). The last of the clustered phosphorylation events (Cluster 3, 36 sites, 13%), represents substrates that are better phosphorylated by M-CDK than S-CDK (Figure 2a,b,e). However, although these substrates were better phosphorylated by M-CDK, most were still well phosphorylated by S-CDK, with only 13 phosphorylation events on 11 substrates (4% of the total sites) failing to reach 30% phosphorylation downstream of S-CDK at the end of the experiment (Table S1).

We conclude that for the majority of substrates the preferences of S-CDK and M-CDK are surprisingly similar, suggesting that the S-cyclin and M-cyclin of the Cyclin-CDK complex do not impose major differences on CDK substrate specificity *in vivo*. Thus, the core CDK control system is predominantly reliant on quantitative levels of generic CDK activity contributed by either S-CDK or M-CDK to phosphorylate substrates (Fig 2b,c), but there are a small number of substrates that rely on qualitative cyclin-specific properties of Cyclin-CDK for efficient phosphorylation (Fig 2b,d,e). The inability of S-CDK to phosphorylate certain substrates within this cluster is likely responsible for S-CDK being unable to substitute for M-CDK. We conclude that the core CDK control is hybrid in nature, predominantly quantitative but with low level qualitative features. The quantitative nature of the CDK core cell cycle control probably reflects the situation operative in primaeval eukaryotes 1.0-1.5 billion years ago, which was likely to have been based on a single CDK.

PP1 restricts S-CDK from executing mitosis

Given the very small differences in CDK substrate phosphorylation between S-CDK and M-CDK, we hypothesised that S-CDK may be able to execute mitosis if its activity is increased against substrates that it phosphorylates less effectively. To investigate this possibility, we examined the effects of four known inhibitory mechanisms that reduce CDK activity *in vivo* (Figure 3a). Firstly, the degradation of S-cyclins targeted by Skp/Cullin/F-box (SCF) ubiquitin ligases, when complexed with the F-box adaptors Pop1 and Pop2, or by the APC/C when complexed with Cdh1[24,25]. Secondly, CDK activity is inhibited by a CDK inhibitor, Rum1[26]. Thirdly, interphase CDK activity is opposed by two phosphatases: Protein Phosphatase 2A (PP2A), and Protein Phosphatase 1 (PP1)[27,28]. Finally, CDK is phosphorylated at residues T14 and Y15 by Wee1 and Myt1, which directly inhibit its catalytic activity[29].

All of these negative regulators were removed genetically, and their efforts on the ability of S-CDK to complete mitosis determined. In the absence of $PP1^{Dis2}$, S-CDK could undergo mitosis, but this was not the case with removal of any of the other negative CDK regulators (Figure 3b, Extended data figure 5). In the absence of PP1, S-CDK expressing cells constructed spindles and degraded S-CDK co-incident with nuclear separation indicating mitotic exit (Figure 3c,d,e), and then proceeded through cytokinesis and cell division (Figure 3f). Mitotic exit was somewhat delayed compared to mitosis driven by M-CDK, and some aberrant divisions were exhibited (Figure 3f, compare to Figure 1i). However, mitosis driven by M-CDK in the absence of PP1 also exhibited some aberrant divisions (Figure 3g). These experiments demonstrate that PP1 plays a significant role in restricting S-CDK from executing a full mitosis.

Centrosomal PP1 specifically restricts S-CDK

PP1 is located throughout the cell but is concentrated at the yeast centrosome (the Spindle Pole Body, or SPB), which organises the mitotic spindle. Given that S-CDK is unable to construct mitotic spindles, we hypothesised that PP1 imposes a CDK activity threshold at the SPB specifically, which S-CDK is unable to surpass. If PP1 at the SPB acts as a S-CDK mitotic restriction factor, then removal of PP1 located at the SPB should be sufficient for a S-CDK mediated mitosis.

PP1 localises to the SPB through the SPB-localised adaptor protein Cut12, which possesses two PP1 binding motifs (Figure 4a), and is evicted from the spindle pole at mitosis through phosphorylation of Cut12 by CDK and the NEK kinase Sid2[30]. We therefore removed PP1 from the centrosome using a mutant of Cut12 that lacks PP1 docking motifs ($Cut12^{\Delta PP1}$, Figure 4a)[30]. This allele was combined with our *in vivo* CDK assay system to determine the influence of centrosomal PP1 in restricting S-CDK mitotic activity. Similar to observations in a wild-type $Cut12^{+}$ background, S-CDK accumulated in the nuclei of cells, followed by synCut3 translocation from the cytoplasm into the nucleus (Figure 4b,c). However, in the absence of SPB-localised PP1, cells were able to undergo mitosis (Figure 4c - bottom row), construct mitotic spindles (Figure 4d), and did not exhibit significant numbers of aberrant division events (Figure 4e). When comparing a M-CDK driven mitosis to a S-CDK driven mitosis in the absence of SPB-localised PP1, there was no difference in the timing of mitosis or in the proportion of cells undergoing division (Figure 4f). We confirmed this result by removing PP1 from the centrosome by mimicking the

phosphorylation events that naturally evict PP1[30], and achieved the same results (Extended data figure 6). These experiments indicate that the S-CDK can execute a proper and timely mitosis as long as the CDK negative regulator PP1 is removed from the centrosome.

Next, we utilised our *in vivo* kinase assay to determine the changes in CDK substrate phosphorylation that lead to this S-CDK driven mitosis. We examined clusters that were phosphorylated in the wild-type strain to examine changes when PP1 is removed from the SPB. As before, the majority of CDK substrates became well phosphorylated by S-CDK, with deletion of centrosomal PP1 having no impact on their average phosphorylation profile (Figure 4g). However, there were some differences in substrates that were poorly phosphorylated by S-CDK (Figure 4h), the two most prominent being the phosphosites *Clp1-T452* and *Plo1-S370*, which are both SPB localised proteins (Figure 4i,j). These phosphosites of Clp1 and Plo1 are reduced in cells driven by S-CDK (Figure 2e) and are increased up to mitotic levels when PP1 is excluded from the SPB. Other substrates that are less phosphorylated by S-CDK were not affected so much by the removal of PP1, demonstrating that centrosomal PP1 alone does not completely equalise S-CDK and M-CDK substrate specificities (Figure 4k, Table S2).

We conclude that some mitotic CDK substrates which are less phosphorylated by S-CDK are restrained from phosphorylation by the presence of PP1 at the centrosome. In the absence of centrosomal PP1, S-CDK is able to phosphorylate substrates essential for mitosis to a mitotically permissible level. These observations support the quantitative view of the CDK cell cycle control because, as well as bringing about S-phase, S-CDK acting alone can also bring about mitosis if its activity is increased by removal of PP1 located at the centrosome. In further support of this concept, we oscillated S-CDK activity using a non-degradable S-CDK$^{\Delta DB}$ modified so it could be inhibited by the inhibitor 1-NmPP1. By varying the levels of exogenously added 1-NmPP1 (Figure 4l) and thus the level of CDK activity in cells, it was possible to drive successive rounds of mitosis and cell division (Figure 4m). Thus, if PP1 is removed from the centrosome, control of cell division can be brought about simply by varying the quantitative level of S-CDK activity.

Discussion

We have shown that the *in vivo* substrate specificities of the major S-CDK and M-CDK in fission yeast are remarkably similar, which is inconsistent with the currently widely accepted qualitative model of core cell cycle control that these CDKs have significant different substrate specificities. For 87% of the 280 CDK phosphosites assayed the S-CDK was either equal to or exceeded the M-CDK in its ability to phosphorylate CDK substrates, the vast majority of which are mitotic. The S-CDK was only less effective than the M-CDK for 13% of the phosphosites, and only 4% had activities less than 30% of the M-CDK. This result is not compatible with a purely qualitative view of core CDK cell cycle control. In contrast, our results support a generally quantitative view of core CDK cell cycle control with a small qualitative element.

The small differences in substrate phosphorylation that are observed are likely to be due to intrinsic dissimilarities between the S-CDK and M-CDK catalytic properties, but boosting S-CDK activity by eliminating the CDK-opposing phosphatase PP1 must allow the phosphorylation of the substrates essential for mitosis. Central to this role of PP1 is its location at the centrosome, because if PP1 is not allowed to dock via Cut12, the S-CDK is able to initiate and complete mitosis in a manner identical to an M-CDK driven mitosis. Thus S-CDK is restricted from executing mitosis by restriction of its activity, particularly by PP1 located at the centrosome.

We conclude that the quantitative view of the core CDK system is the dominating feature that brings about the control and temporal order of S-phase and mitosis, with rising overall CDK activity contributed by both S-CDK or M-CDK serving as the core cell cycle organising principle. However, there are small qualitative differences in substrate specificity between Cyclin-CDK complexes that are essential for cell cycle control, which include a PP1 based regulatory process located at the mitotic spindle forming centrosome. This reconciles the two contrasting views of CDK cell cycle control, which we propose is hybrid with a predominantly quantitative nature and a small qualitative influence. This view of CDK cell cycle control can be tested in other eukaryotes including mammalian cells using the *in vivo* CDK assay and methodology described here. Our conclusions are likely to be of relevance to core cell cycle control in other eukaryotes, given the extensive degree of functional redundancy and plasticity for CDKs and cyclins reported other eukaryotic species[10-12,20]. However, the more complex control of the cell cycle required in multicellular eukaryotes built on interacting tissues and organs may involve more qualitative regulatory features added to the core regulation we describe here.

Main References

1 Hochegger, H., Takeda, S. & Hunt, T. Cyclin-dependent kinases and cell-cycle transitions: does one fit all? *Nat Rev Mol Cell Biol* **9**, 910-916, doi:10.1038/nrm2510 (2008).

2 Loog, M. & Morgan, D. O. Cyclin specificity in the phosphorylation of cyclin-dependent kinase substrates. *Nature* **434**, 104-108, doi:10.1038/nature03329 (2005).

3 Morgan, D. O. *The cell cycle : principles of control*. (Published by New Science Press in association with Oxford University Press ;Distributed inside North America by Sinauer Associates, Publishers, 2007).

4 Alberts, B. *Molecular biology of the cell*. Sixth edition. edn, (Garland Science, Taylor and Francis Group, 2015).

5 Koivomagi, M. *et al.* Dynamics of Cdk1 substrate specificity during the cell cycle. *Mol Cell* **42**, 610-623, doi:10.1016/j.molcel.2011.05.016 (2011).

6 Pagliuca, F. W. *et al.* Quantitative proteomics reveals the basis for the biochemical specificity of the cell-cycle machinery. *Mol Cell* **43**, 406-417, doi:10.1016/j.molcel.2011.05.031 (2011).

7 Stern, B. & Nurse, P. A quantitative model for the cdc2 control of S phase and mitosis in fission yeast. *Trends Genet* **12**, 345-350 (1996).

8 Uhlmann, F., Bouchoux, C. & Lopez-Aviles, S. A quantitative model for cyclin-dependent kinase control of the cell cycle: revisited. *Philos Trans R Soc Lond B Biol Sci* **366**, 3572-3583, doi:10.1098/rstb.2011.0082 (2011).

9 Swaffer, M. P., Jones, A. W., Flynn, H. R., Snijders, A. P. & Nurse, P. CDK Substrate Phosphorylation and Ordering the Cell Cycle. *Cell* **167**, 1750-1761 e1716, doi:10.1016/j.cell.2016.11.034 (2016).

10 Kalaszczynska, I. *et al.* Cyclin A is redundant in fibroblasts but essential in hematopoietic and embryonic stem cells. *Cell* **138**, 352-365, doi:10.1016/j.cell.2009.04.062 (2009).

11 Geng, Y. *et al.* Cyclin E ablation in the mouse. *Cell* **114**, 431-443, doi:10.1016/s0092-8674(03)00645-7 (2003).

12 Kozar, K. *et al.* Mouse development and cell proliferation in the absence of D-cyclins. *Cell* **118**, 477-491, doi:10.1016/j.cell.2004.07.025 (2004).

13 Schwob, E. & Nasmyth, K. CLB5 and CLB6, a new pair of B cyclins involved in DNA replication in Saccharomyces cerevisiae. *Genes Dev* **7**, 1160-1175, doi:10.1101/gad.7.7a.1160 (1993).

14 Fisher, D. L. & Nurse, P. A single fission yeast mitotic cyclin B p34cdc2 kinase promotes both S-phase and mitosis in the absence of G1 cyclins. *EMBO J* **15**, 850-860 (1996).

15 Hayles, J., Fisher, D., Woollard, A. & Nurse, P. Temporal order of S phase and mitosis in fission yeast is determined by the state of the p34cdc2-mitotic B cyclin complex. *Cell* **78**, 813-822, doi:10.1016/s0092-8674(94)90542-8 (1994).

16 Santamaria, D. *et al.* Cdk1 is sufficient to drive the mammalian cell cycle. *Nature* **448**, 811-815, doi:10.1038/nature06046 (2007).

17 Zarzov, P., Decottignies, A., Baldacci, G. & Nurse, P. G(1)/S CDK is inhibited to restrain mitotic onset when DNA replication is blocked in fission yeast. *EMBO J* **21**, 3370-3376, doi:10.1093/emboj/cdf346 (2002).

18 Obara-Ishihara, T. & Okayama, H. A B-type cyclin negatively regulates conjugation via interacting with cell cycle 'start' genes in fission yeast. *EMBO J* **13**, 1863-1872 (1994).

19 Hegarat, N. *et al.* Cyclin A triggers Mitosis either via the Greatwall kinase pathway or Cyclin B. *EMBO J* **39**, e104419, doi:10.15252/embj.2020104419 (2020).

20 Cross, F. R., Yuste-Rojas, M., Gray, S. & Jacobson, M. D. Specialization and targeting of B-type cyclins. *Mol Cell* **4**, 11-19, doi:10.1016/s1097-2765(00)80183-5 (1999).

21 Lorca, T. *et al.* Cyclin A-cdc2 kinase does not trigger but delays cyclin degradation in interphase extracts of amphibian eggs. *J Cell Sci* **102 (Pt 1)**, 55-62 (1992).

22 Pickering, M., Magner, M., Keifenheim, D. & Rhind, N. The fission yeast S-phase cyclin Cig2 can drive mitosis. *Genetics* **217**, 1-12, doi:10.1093/genetics/iyaa002 (2021).

23 Patterson, J. O., Basu, S., Rees, P. & Nurse, P. CDK control pathways integrate cell size and ploidy information to control cell division. *Elife* **10**, doi:10.7554/eLife.64592 (2021).

24 Blanco, M. A., Sanchez-Diaz, A., de Prada, J. M. & Moreno, S. APC(ste9/srw1) promotes degradation of mitotic cyclins in G(1) and is inhibited by cdc2 phosphorylation. *EMBO J* **19**, 3945-3955, doi:10.1093/emboj/19.15.3945 (2000).

25 Yamano, H. *et al.* Requirement of the SCFPop1/Pop2 Ubiquitin Ligase for Degradation of the Fission Yeast S Phase Cyclin Cig2. *J Biol Chem* **279**, 18974-18980, doi:10.1074/jbc.M311060200 (2004).

26 Moreno, S. & Nurse, P. Regulation of progression through the G1 phase of the cell cycle by the rum1+ gene. *Nature* **367**, 236-242, doi:10.1038/367236a0 (1994).

27 Mochida, S., Ikeo, S., Gannon, J. & Hunt, T. Regulated activity of PP2A-B55 delta is crucial for controlling entry into and exit from mitosis in Xenopus egg extracts. *EMBO J* **28**, 2777-2785, doi:10.1038/emboj.2009.238 (2009).

28 Grallert, A. *et al.* A PP1-PP2A phosphatase relay controls mitotic progression. *Nature* **517**, 94-98, doi:10.1038/nature14019 (2015).

29 Gould, K. L. & Nurse, P. Tyrosine phosphorylation of the fission yeast cdc2+ protein kinase regulates entry into mitosis. *Nature* **342**, 39-45, doi:10.1038/342039a0 (1989).

30 Grallert, A. *et al.* Removal of centrosomal PP1 by NIMA kinase unlocks the MPF feedback loop to promote mitotic commitment in S. pombe. *Curr Biol* **23**, 213-222, doi:10.1016/j.cub.2012.12.039 (2013).

Materials And Methods

S. pombe genetics and cell culture

Fission yeast media and growth conditions were described previously[31]. Unless otherwise stated, all experiments were conducted in yeast extract (YE) media supplemented with adenine, leucine, histidine and uracil to a final concentration of 0.15 g/L. Cells were grown at 25°C unless stated otherwise. All experiments were performed with cells in exponential growth, defined as 2.5 - 10 x 10^6 cells/ml. The temperature sensitive Cdk1 allele used was *cdc2-M26*. To induce the tetracycline-dependent promoter, anhydrotetracycline hydrochloride (Sigma) dissolved in DMSO was added to a final concentration of 0.3125 µg/ml. Vehicle concentration whilst using 1-NMPP1 or tetracycline was not allowed to exceed

0.1% v/v of total culture volume to prevent DMSO-mediated toxicity. Strains were constructed either by genetic crossing or by direct transformation as previously described [31]. All strains were checked for correct genotypes by colony PCR prior to use. All strains used, and plasmids used to construct strains, are given in Supplementary Table 3.

Fluorescence microscopy

All live cell fluorescence microscopy was performed using a Nikon Ti12 inverted microscope with Perfect Focus System and Okolab environmental chamber, and a Prime sCMOS camera (Photometrics). The microscope was controlled with Micro-Manager v2.0 software (Open-imaging) [32]. Fluorescence excitation was performed using a SpectraX LED light engine (Lumencor) fitted with standard filters: 470/24 for imaging sfGFP; and 575/25 for imaging mCherry; with either a dual-edge ET-eGFP/mCherry dichroic beamsplitter, Chroma 59022bs, or a BrightLine® quad-edge dichroic beamsplitter, Semrock FF409-493-573-652. Emission filters were as follows: Chroma, ET - EGFP single-band bandpass filter ET525_50m for imaging sfGFP; and Semrock, 641/75 nm BrightLine® single-band bandpass filter FF02_641_75 for imaging mCherry. Images were taken using a 100X Plan Apochromat oil-immersion objective (NA 1.45) at 25 °C. ImageJ software (NIH) was used to measure pixel intensity, adjust brightness and contrast and render maximum projection images [33]. Unless otherwise stated, all images represent a single Z-slice across the medial focal plane of cells. For any given figure panel, the same pixel range has been applied to all images from the same channel, thus making images in the same channel comparable.

Cell cycle progression determination

To score for nuclear division and cell septation indices, 4 µl of cell suspension was heat fixed at 70 °C before addition of DAPI to monitor DNA, and Calcofluor to monitor septum formation. For determination of these indices, samples were imaged on a Zeiss Axioskop, 63x/1.4 NA objective or a Nikon Ti12 inverted microscope with Perfect Focus System, 100x/1.45 NA objective (Photometrics). Spindle formation and nuclear enrichment indices were obtained using images from live-cell widefield imaging. Spindle formation was scored as positive if there was a clear linear trace of sfGFP fluorescence between SPB-like structures. To check for nuclear enrichment of synCut3-mCherry and Cyclin-Cdk1-sfGFP, the mean pixel value of a circle encompassing the nucleus was compared to the mean pixel value of a circle of equal area drawn in the cytoplasm. If the nuclear mean value was 1.5x the cytoplasmic value (or higher), then this was classed as nuclear enrichment. All nuclear enrichment indices, cell cycle progression indices, and spindle formation indices were conducted on 100 cells per timepoint.

Protein Extraction and Western Blotting

Protein was extracted from cell culture initially by quenching with 100% w/v ice-cold trichloroacetic acid to a final concentration of 10%. Cells were stored on ice for 20 minutes, pelleted at 3000 x *g*, and washed in acetone before storage at -80 °C. After storage, pellets were resuspended in lysis buffer (8M Urea, 50 mM ammonium bicarbonate, 1x cOmplete mini EDTA-free protease inhibitor + 1x phosSTOP phosphatase inhibitor cocktail). Roughly 1.2 mL of 0.4 mm acid-washed glass beads were then added to

suspensions, which were subject to three rounds of beating at 5.5 m/s for 30 s (FastPrep120). Cell debris was then pelleted at 16,000 x g for 5 minutes, and supernatant stored as whole-cell protein sample at -80 °C. Protein detection by western blotting was performed for Cig2 using 1:500 α-Cig2 (mouse monoclonal) (abcam, CIG 3A11/5, Cat#: ab10881) blocked with 5% milk in TBS-Tween. Secondary antibody used was 1:5000 goat anti-mouse (STAR120P, AbD SeroTEC). Signal was detected using SuperSignal West Femto Maximum Sensitivity Substrate (34095, Life Technologies) and imaged on an Amersham Imager 600.

Tandem mass tag proteomics

Each protein sample (400 µg) was reduced with 5 mM dithiothreitol (DTT) for 25 min at 56 °C, alkylated with 10 mM iodoacetamide for 30 min at room temperature in the dark and then quenched with 7.5 M DTT. Samples were digested using SP3 on-bead methodology[34] with the variation that 50 mM HEPES (pH 8.5) was used in place of ammonium bicarbonate. Briefly, proteins were bound to the SP3 beads (10:1 beads:protein (w/w)) in 50 % ethanol (v/v) and then washed three times in 80 % ethanol, prior to resuspension in 50 mM HEPES (pH 8.5) with 1:40 (trypsin:protein (w/ w)) overnight at 37 °C. The digested samples were arranged in sets of 16 and labelled using the TMTpro 16plex Isobaric Label Reagent Set (Thermo Fisher), as per the manufacturer's instructions. Following labelling and mixing, multiplexed samples were desalted using a C18 SepPak column. Phosphopeptide enrichment was performed by Sequential Enrichment from Metal Oxide Affinity Chromatography (SMOAC, Thermo Fisher) with initial enrichment using the HighSelect TiO2 Phosphopeptide Enrichment Kit followed by the HighSelect Fe-NTA Phosphopeptide Enrichment Kit (both Thermo Scientific) for the non-bound flow through fractions. Phosphopeptides and non-bound flow through fractions were desalted and fractionated using the High pH Reversed-Phase Peptide Fractionation Kit (Pierce) and analysed on an Orbitrap Fusion Lumos mass spectrometer (Thermo Fisher) coupled to an UltiMate 3000 HPLC system for online liquid chromatographic separation. Each run consisted of a 3 h gradient elution from a 75 µm × 50 cm C18 column. MaxQuant (version 1.6.14.0) was used for all data processing. The data were searched against a PomBase[35] extracted *S. pombe* proteome FASTA file. Default MaxQuant parameters were used with Phospho(STY) being added as a variable modification, MaxQuant output files were imported into Perseus (version 1.6.14.0).

Mass spectrometry data analysis

MaxQuant (version 1.5.0.13) was used for all data processing. The data was searched against a UniProt extracted *Schizosaccharomyces pombe* proteome FASTA file, amended to include common contaminants. Default MaxQuant parameters were used with the following adjustments: Phospho(STY) was added as a variable modification (for the phosphopeptide enriched samples), MaxQuant output files were imported into Perseus (version 1.6.4.7) for further data analysis. The same phosphosite with different phosphorylation multiplicity was considered to be a separate phosphorylation event. Known CDK sites were excluded if they displayed consistent aberrant phosphorylation behaviour upon Cyclin-CDK induction. This led to ~9% data loss. Prior to data representation, up to a single aberrant point per

phosphosite was removed per trace. No individual points were removed for hierarchical clustering. For the generation of heatmaps, clustering was conducted using L1 distance with initial k-means clustering (Perseus 1.6.4.7).

Data representation

All statistical tests were conducted using GraphPad Prism 7 or Prism 8. The central point of all datapoints gives the mean, with whiskers delimiting either the 95% CI (for phosphoproteomic data) or SD/SEM for all other data. Where error bars are not present, they are smaller than the size of the datapoint.

Method References

31 Moreno, S., Klar, A. & Nurse, P. Molecular genetic analysis of fission yeast Schizosaccharomyces pombe. *Methods Enzymol* **194**, 795-823, doi:10.1016/0076-6879(91)94059-l (1991).

32 Edelstein, A. D. *et al.* Advanced methods of microscope control using muManager software. *J Biol Methods* **1**, doi:10.14440/jbm.2014.36 (2014).

33 Schindelin, J. *et al.* Fiji: an open-source platform for biological-image analysis. *Nat Methods* **9**, 676-682, doi:10.1038/nmeth.2019 (2012).

34 Hughes, C. S. *et al.* Single-pot, solid-phase-enhanced sample preparation for proteomics experiments. *Nat Protoc* **14**, 68-85, doi:10.1038/s41596-018-0082-x (2019).

35 Lock, A. *et al.* PomBase 2018: user-driven reimplementation of the fission yeast database provides rapid and intuitive access to diverse, interconnected information. *Nucleic Acids Res***47**, D821-D827, doi:10.1093/nar/gky961 (2019).

Declarations

Acknowledgements

We thank Jessica Greenwood and Clovis Basier for their comments on the manuscript. This work was supported by the Francis Crick Institute which receives its core funding from Cancer Research UK (FC01121), the UK Medical Research Council (FC01121), and the Wellcome Trust (FC01121). In addition, this work was supported by the Wellcome Trust Grant to PN [grant number 214183 and 093917], The Lord Leonard and Lady Estelle Wolfson Foundation, and Woosnam Foundation.

Author Contributions

S.B. and P.N. initiated the study. S.B. generated reagents, designed and performed experiments, and conducted data analysis. A.W.J. performed mass spectrometry and data analysis. S.B. and P.N. wrote the manuscript.

Additional Information

Supplementary Information is available for this paper

Competing Interests

The authors declare no competing interests.

Data and Reagent Availability Statement

The mass spectrometry proteomics data have been deposited to the ProteomeXchange Consortium via the PRIDE partner repository with the dataset identifier PXD029073. Correspondence and requests for materials should be addressed to Souradeep Basu, at saz.basu@crick.ac.uk.

Figures

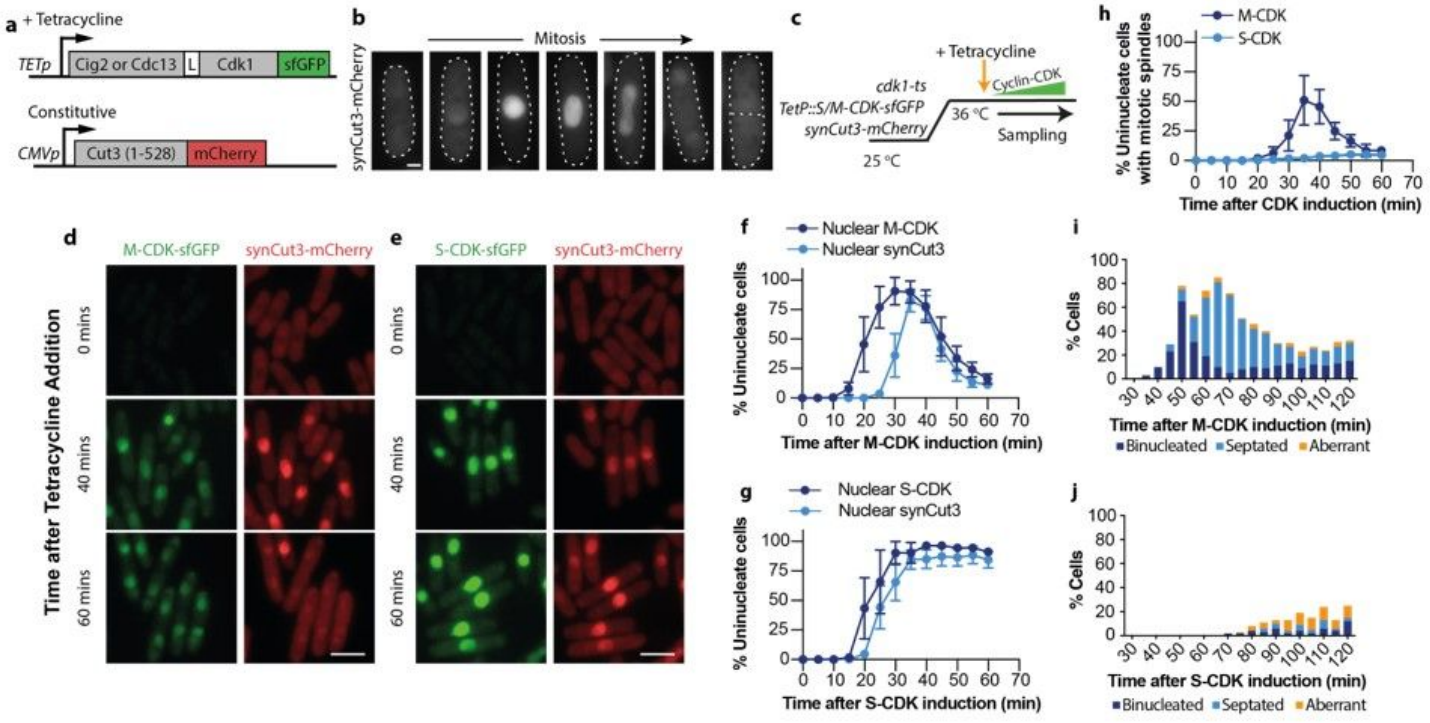

Figure 1

S-CDK can drive mitotic entry, but cannot complete mitosis. a Schematic of dual promoter system. TETp: tetracycline-dependent promoter; CMVp: constitutive CMV promoter. b Example images of cells expressing synCut3-mCherry during mitosis. Scale bar = 2μm. c Experimental schematic for panels (d)-(j).

d/e Representative images following induction of: M-CDK-sfGFP (d); or S-CDK-sfGFP (e). Scale bar = 10μm. f/g Percentage of uninucleate cells with nuclear M-CDK-sfGFP (f) or S-CDK-sfGFP (g) and nuclear synCut3-mCherry, as a percentage of all cells. Points give mean, error bars give SD. 100 cells/timepoint. n=6. h Percentage of uninucleate cells with spindles, as a percentage of all cells. Points give mean, error bars delimit SD. 100 cells/timepoint. n=3. i/j Quantitation of mitotic and post-mitotic events during a longer expression of M-CDK-sfGFP (i) or S-CDK (j). n=100 cells/timepoint.

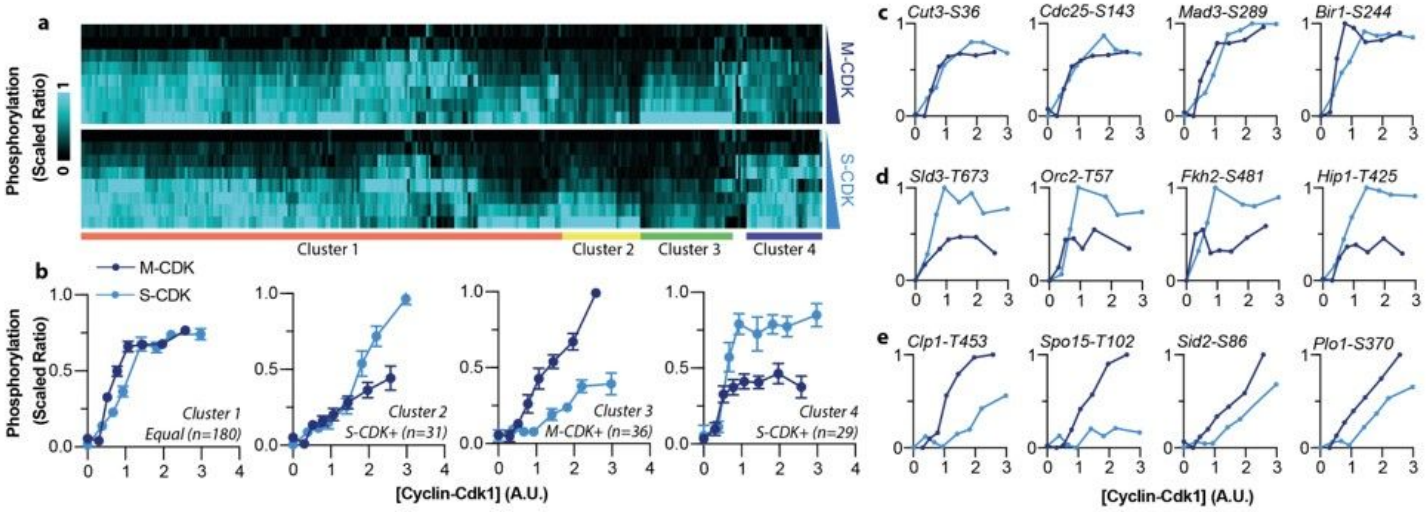

Figure 2

Global phosphorylation of S-CDK and M-CDK complexes a Heatmap of 280 detected CDK phosphorylation events that showed consistent phosphorylation behaviour. Sites are hierarchically clustered into four distinct groups. 5 sites were not clustered. b Average phosphorylation behaviour for each of the four detected clusters, labelled in panel (b). Points = mean, error bars give 95% CI. c,d,e Representative substrates from Cluster 1(c), Clusters 2/4 (d), and Cluster 3 (e).

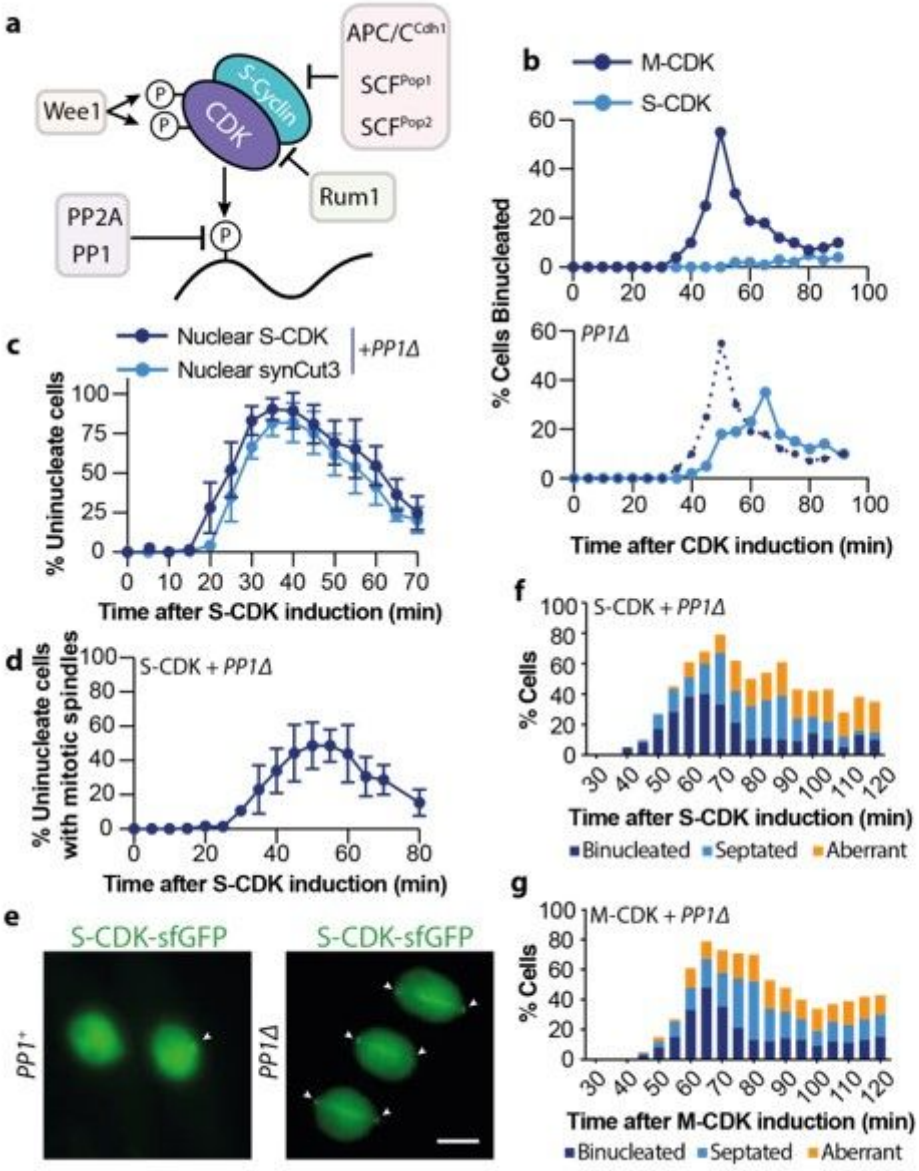

Figure 3

PP1 restricts S-CDK from executing mitosis a Negative regulators of S-CDK, and their point of action. b Upper: Binucleation index after induction of S-CDK-sfGFP and M-CDK-sfGFP. Lower: Binucleation index of a S-CDK-sfGFP induction in PP1Dis2Δ. M-CDK data replicated from upper panel. 100 cells/timepoint. c Percentage of uninucleate cells with nuclear S-CDK-sfGFP in combination with nuclear synCut3-mCherry, given as a percentage of all cells. Points give mean, error bars give SD. 100 cells/timepoint, n=6. d Percentage of uninucleate cells with spindles, given as a percentage of all cells, in an S-CDK induction in the absence of PP1. Points give mean, error bars delimit SD. 100 cells/timepoint. n=3 e Example images of mitotic cells in either a PP1+ or PP1Dis2Δ background. Spindle poles are marked with arrows. f,g Quantitation of mitotic and post-mitotic events during a longer expression of M-CDK-sfGFP (f) or S-CDK-sfGFP (g) in PP1Dis2Δ. from Calcofluor and DAPI staining fixed cells. 100 cells/timepoint.

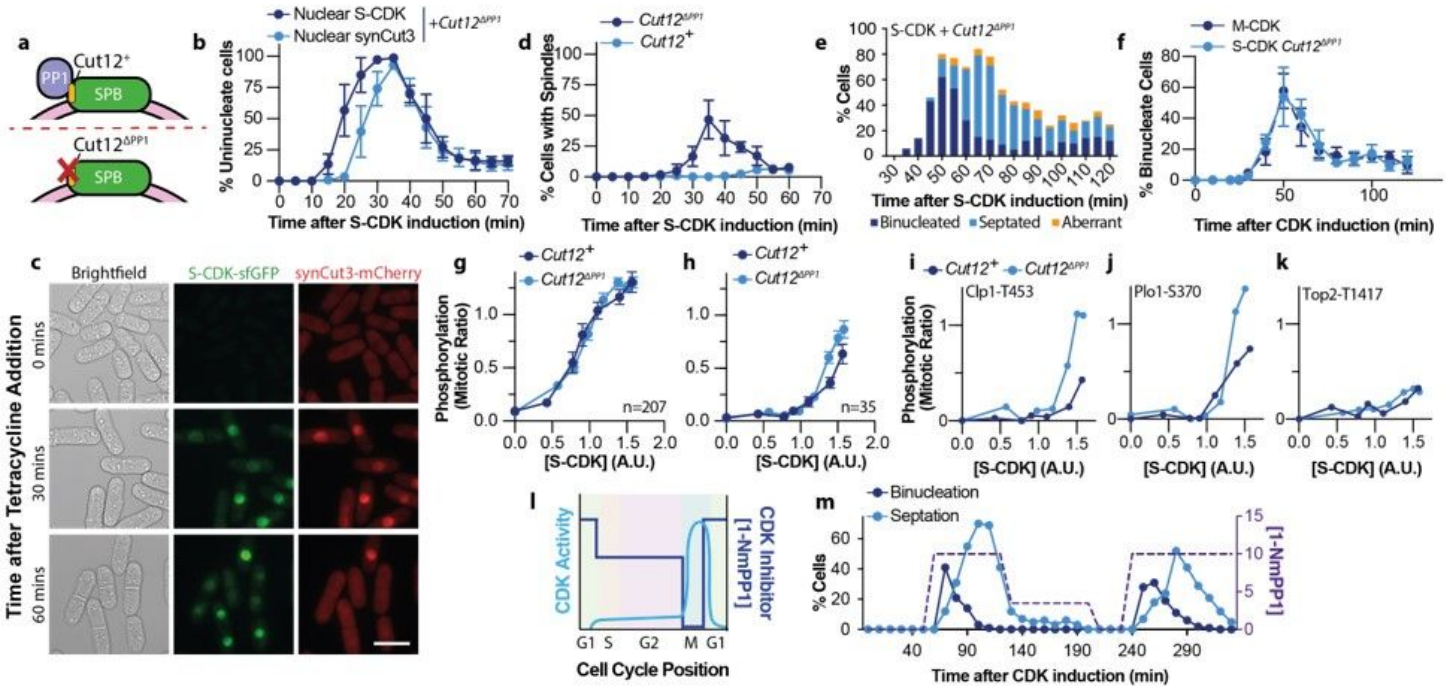

Figure 4

PP1 at the SPB alone restricts S-CDK from executing mitosis a PP1-SPB docking through Cut12. Cut12ΔPP1 possesses mutations in two PP1 binding motifs. b Percentage of uninucleate cells with nuclear S-CDK-sfGFP in combination with nuclear synCut3-mCherry, given as a percentage of all cells. Points give mean, error bars give SEM. 100 cells/timepoint, n=3. c Representative images of cells following induction of S-CDK-sfGFP. Scale bar = 10 μm d Percentage of uninucleate cells with spindles, as a percentage of all cells, in an S-CDK induction +/- Cut12ΔPP1. Points give mean, error bars delimit SD. 100 cells/timepoint, n=3 e Quantitation of mitotic and post-mitotic events during a longer expression of S-CDK with Cut12ΔPP1. 100 cells/timepoint. f Binucleation index after S-CDK-sfGFP induction in the Cut12ΔPP1 background or M-CDK-sfGFP in Cut12+. Points give mean, error bars give SEM. 100 cells/datapoint, n=3. g/h Average substrate phosphorylation profiles of the phosphorylated (g) and poorly phosphorylated (h) substrate clusters by S-CDK in Cut12+ or Cut12ΔPP1. i/j/k Example substrate phosphorylation profiles of substrates better (i/j) or equally (k) phosphorylated by S-CDK in Cut12ΔPP1 l Schematic of inhibitor enforced oscillations of CDK activity. m Binucleation and septation indices (left y-axis) after S-CDK induction and [1-NmPP1] (right y-axis). 100 cells/timepoint.

Supplementary Files

This is a list of supplementary files associated with this preprint. Click to download.

- ExtendedFiguresLegends.docx
- TableS1CDKsiteclassificationuponSCDKandMCDKinduction.xlsx

- TableS2InfluenceofCut12XXPP1onhypophosphorylatedSCDKsites.xlsx
- TableS3StrainsandPlasmids.xlsx